Influence of Hall thruster operating mode on plasma sheath location

IEPC-2017-87

Presented at the 35th International Electric Propulsion Conference
Georgia Institute of Technology • Atlanta, Georgia • USA
October 8 – 12, 2017

Andrey S. Shashkov[1]
Keldysh Research Centre, Moscow, 125438, Russia

Moscow Institute of Physics and Technology (State University), Moscow, 141700, Russia

and

Alexander S. Lovtsov[2]

Keldysh Research Centre, Moscow, 125438, Russia

Elaboration of magnetically shielded Hall thrusters requires specification of the plasma sheath location along the discharge channel. The location of the plasma sheath determines erosion belts location and thruster's maximum throughput consequently. For a Hall thruster with wide throttle ratio the location of the plasma sheath in each operating mode could vary significantly, which makes it difficult to provide necessary throughput for multi-mode operation. In this article, the shift of the plasma sheath location caused by the change of operating mode is studied with the help of both numerical and experimental methods. Numerical investigation was conducted with 1D3V hybrid-PIC simulations. Experimental research was carried out with electrical probe measurements on KM-88 Hall thruster. According to the results of the study, the plasma sheath could move upstream significantly with gas flow rate and magnetic field increase. Also, it was proved that magnetic field gradient increase shifts plasma sheath downstream significantly. Moreover, both numerical and experimental investigations indicate that the plasma sheath could move significantly when oscillation mode changes. The impact of the oscillations on plasma sheath location is discussed in the paper.

Nomenclature

A = Hall thruster channel crossection
B_{max} = Maximum magnetic field on the middle line

---

[1] Research Scientist, Department of Electrophysics, shashkov@phystech.edu.
[2] Head of Department, Department of Electrophysics.

E_x = Axial electric field
e = Elementary charge
I_d = Discharge current oscillations
$\sim I_d$ = Discharge current oscillations amplitude
k = Boltzmann constant
l = Discharge channel length
M = Xenon atom mass
m = Electron mass
$\dot{m}_a$ = Gas flow rate
N = Neutral atoms concentration
N^* = Excited neutral atoms concentration
n = Electron concentration
n_i^+ = Singly charge ion concentration
n_i^{++} = Doubly charge ion concentration
P_{ew} = Electron-wall energy loss rate
R, r = Outer and inner radiuses
T = Electron temperature
t = Time
u_x = Electron axial velocity
u_θ = Electron azimuthal velocity
${U_x}^+$ = Singly charged ions axial velocity
${U_x}^{++}$ = Doubly charged ions axial velocity
x = Axial coordinate
$\beta_{0,1,2,3}$ = Single, double, secondary and stepwise ionization collision rates
$\beta_{elastic}, \beta_{excit}$ = Elastic and excitation collision rates
$\gamma_{0,1,2,3}, \gamma_{excit}$ = Single, double, secondary, stepwise ionization losses and excitation losses
ε = Full electron energy
μ_{eff} = Effective electron mobility
ν_i, ν_e = Ionization collision frequency and total electron momentum transfer frequency
$\nu_{coulomb}, \nu_{ew}, \nu_{ano}$ = Coulomb, electron-wall and the anomalous diffusion collision frequencies
σ = Secondary electron emission coefficient
Φ_w = Radial sheath potential
ϕ = Plasma potential
ϕ_{fl} = Floating potential
$\Delta\phi$ = Discharge voltage
ω = Electron cyclotron frequency

I. Introduction

Ceramic insulators erosion is one of the vital processes that reduce the Hall thruster operating lifetime. The pace of the erosion is determined by ionization and acceleration region location. Therefore, numerous studies were conducted to find a way to influence the plasma sheath location. As a result, it was revealed that the magnetic field has the biggest influence on the plasma sheath location[1,2] and a high life design scheme was suggested[3]. Qualification Life Test of the BPT-4000 Hall thruster showed that the erosion of the acceleration channel had practically ceased after about 5600 hours of operation[4]. The phenomena was investigated numerically with Hall2De code[5]. The magnetic field aligned mesh plasma solver revealed that in the given BPT-4000 thruster's geometry and magnetic field configuration plasma potential along the thruster's acceleration channel was practically equal to anode plasma potential. Lack of the plasma potential drop along the ceramics led to insufficient ion bombardment of the acceleration channel and that stopped the erosion. The revelation changed Hall thrusters' magnetic system and ceramics design, and thrusters with such magnetic configuration were named "magnetically shielded", as it was offered in Ref. 5.

Another trend in Hall thrusters design is development of thrusters with wide throttle ratio. In case of success, these thrusters could accomplish various types of tasks. For example, HERMeS, one of the most recent "magnetically shielded" thrusters, has power throttling ratio 21:1 and discharge current ratio 16:1[6]. Wide power throttling ratio allows to use HERMeS both for human space missions and on small science satellites. Wide discharge current ratio allows HERMeS to operate both in high thrust and high specific impulse regimes. However, it was shown in the M. Belikov's et al. paper[7] that the plasma sheath changes location whenever thruster's operating mode is being changed. Consequently, the magnetic field configuration needs correction to conserve the "magnetic shielding" when the operating conditions change within the throttling ratio.

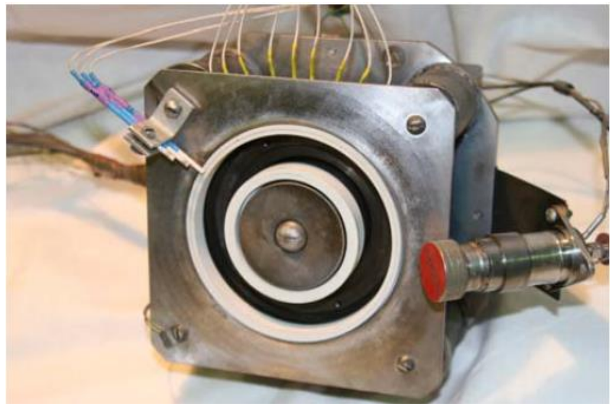

Figure 1. KM-88 thruster equipped with 12 Langmuir probes.

Experimental study of the plasma sheath location for each thruster is unreasonably expensive; it takes a considerable amount of time, and is hardly technically possible. The aim of this paper is to elucidate general tendencies in plasma sheath location shift driven by the changes in Hall thruster operating conditions within the throttling ratio. The research was carried out using both experimental and numerical methods. The experimental conditions and facilities for the investigation of the plasma sheath location are presented in Section II. Section III focuses on the numerical investigation of the plasma sheath, the model used in simulations and the results of the simulations. Section IV compares and discusses the dependencies of the plasma sheath shift on gas flow rate, magnetic field on the middle-line, and discharge voltage obtained both experimentally and numerically. The influence of the discharge current oscillations on the plasma sheath shift is also discussed in the last Section.

II. Experiment

The research was carried out in the KVU-90 vacuum chamber in Keldysh Research Centre[8]. For their studies the authors used a laboratory model of 1.5 kW KM-88 thruster with the middle-line diameter equal to 88 mm. KM-88 thruster equipped with Langmuir probes is presented in the Fig. 1. The ceramic insulators were made of BGP-10 ceramics and had non-magnetic-shielding geometry. Such geometry was set to study experimentally the plasma sheath location in a Hall thruster channel with the help of 12 Langmuir probes. 9 of the probes had radiuses of 0.5 mm and were flush-mounted with the outer ceramic insulator at the distance of 1 mm from each other in the axial direction. These 9 probes were separated by 7.5° in the azimuthal direction to minimize their mutual influence on each other. Other 3 probes had radiuses of 1 mm and were located at 3, 9, and 15 mm distance from the thruster's exit plane. These 3 probes were separated by 5 mm from each other in the radial direction and had no separation in the azimuthal direction. More detailed description and illustration of the probes location could be found in Ref. 7. Langmuir probes were shown to have no influence on the KM-88 parameters. The floating potential was obtained with 12 probes in each operating condition.

Besides the floating potential and thruster parameters the discharge current oscillations were measured for each operating condition with the Hall sensor CM-I-H Pearson Coil with the maximum frequency of 100 kHz and the oscillograph ARBG-4113/6.

The vital distinction between our experiment and the experiment in Ref. 7 is that only one operating parameter was changed simultaneously, while the others were fixed. 3 different parameters were changed: the absolute value of the magnetic field, gas flow rate and discharge current. In particular, these 3 parameters could be changed within the thruster's throttling ratio. All the operating conditions that were studied with the Langmuir probes are presented in Tables 1-3. Table 1 presents the operating modes with different gas flow rate, Table 2 contains the regimes with different maximum magnetic field on the middle-line, and Table 3 illustrates the regimes with different discharge voltages only.

Thus, the floating potential distributions were obtained for each operating mode. The distributions do not show clearly the plasma sheath location. However, the decline rate of the floating potential shows the direction of the plasma sheath shift.

The results of the experiment are presented in Section IV. The probe №3 was damaged when the thruster was being mounted into the vacuum chamber, which resulted in undervalued floating potential on it. However, that fact did not affect the shape of the floating potential distribution and did not deform the trend.

Table 1. Operating conditions for studying gas flow rate influence on the plasma sheath location.

№		1	2	3	4	5	6
Gas flow rate	$\dot{m}_a$, mg/s	1,5	2	2,5	3	3,5	4
Discharge voltage	$\Delta\phi$, V	300	300	300	300	300	300
Discharge current	I_d, A	1,35	1,74	2,2	2,79	3,17	3,67
Amplitude of the discharge current oscillations	$\sim I_d$, A	0,48	0,3	0,4	0,6	1,06	1,2
Maximum magnetic field on the middle-line	B_{max}, Gs	214	214	214	214	214	214

Table 2. Operating conditions for studying magnetic field influence on the plasma sheath location.

№		7	8	9	10	11	12
Gas flow rate	$\dot{m}_a$, mg/s	3	3	3	3	3	3
Discharge voltage	$\Delta\phi$, V	300	300	300	300	300	300
Discharge current	I_d, A	3,06	3,06	2,9	2,85	2,85	2,85
Amplitude of the discharge current oscillations	$\sim I_d$, A	1,86	1,3	0,4	0,35	0,32	0,33
Maximum magnetic field on the middle-line	B_{max}, Gs	167	191	214	238	261	284

Table 3. Operating conditions for studying discharge voltage influence on the plasma sheath location.

№		13	14	15	16	17	18	19
Gas flow rate	$\dot{m}_a$, mg/s	3	3	3	3	3	3	3
Discharge voltage	$\Delta\phi$, V	250	300	350	400	450	500	550
Discharge current	I_d, A	2,71	2,76	2,77	2,78	2,88	3,07	3,15
Amplitude of the discharge current oscillations	$\sim I_d$, A	0,15	0,23	0,47	0,85	0,7	0,8	0,7
Maximum magnetic field on the middle-line	B_{max}, Gs	261	261	261	261	261	261	261

III. Numerical model

A Numerical model description

Since 19 different operating conditions were examined with the probes, at least 19 different numerical calculations should be carried out to validate experimental results. Conducting this number of studies with 2D3V model like Hall2De[5], would require lots of computational time. In addition, the axial position of the ionization region could be studied in one-dimensional formulation. Therefore, numerical simulations in this work were conducted with 1D3V hybrid-PIC model, described in details in Ref. 9. The similar models are the 1D hybrid-kinetic model by Hara at al[10], 1D hydrodynamic model by Rostler[11] and 1D hybrid model by Garrigues at al.[12] Compared to the mentioned analogues, this model takes into account neutral-wall collisions inside of the channel and handles correctly the macroparticles behavior in absence of walls outside of the channel. It also includes the inner magnetic field, ion-neutral recharge, second, double and stepwise ionization, excitation and relaxation of neutral particles. To model anomalous mobility authors used two-region Bohm model with coefficients 1/160 inside the channel and 1/40 outside the channel. In Ref. 9 authors show that the results of the simulations of both thruster parameters and ionization breathing mode oscillations are in a good agreement with the experimental data for studied in that paper KM-88 and KM-60 thrusters.

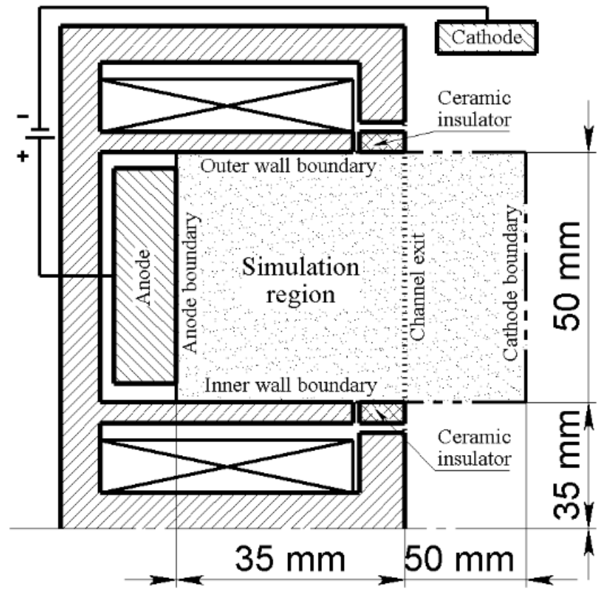

Figure 2. The simulation region scheme.

The simulation region consisted of a ring-shape cylinder with inner radius of 35 mm, outer radius of 50 mm, channel length of 35 mm and simulation region length of 50 mm (Fig. 2). The exit plane was set at coordinate $x=0$.

The chosen hybrid formulation assumes hydrodynamic electron component and 1D3V kinetic ion and neutral components. To decrease PIC method statistical noise the authors used the method of controlling macroparticles number described in Ref. 9.

Initial equation system for the electrons includes quasineutrality condition, continuity, momentum, and energy equations. With doubly charged ions accounted the quasineutrality condition gives:

$$n = n_i^+ + 2n_i^{++}, \tag{1}$$

where $n_i^+ = \int f_i^+(x, U_x, t)dU_x$ is the singly charged ions density, $n_i^{++} = \int f_i^{++}(x, U_x, t)dU_x$ is the doubly charged ions density, f_i^+ and f_i^{++} are the singly and doubly charged ions velocity distribution functions obtained from PIC simulation, x and t are the axial coordinate and time.

In case there are enough macroparticles of heavy species per cell, the continuity equations for the electrons and heavy species could be written as:

$$\frac{\partial n}{\partial t} + \frac{\partial n u_x}{\partial x} = \nu_i n, \tag{2}$$

$$\frac{\partial n_i^+}{\partial t} + \frac{\partial n_i^+ {U_x}^+}{\partial x} = \beta_0 N n + \beta_3 N^* n, \tag{3}$$

$$\frac{\partial n_i^{++}}{\partial t} + \frac{\partial n_i^{++} {U_x}^{++}}{\partial x} = 2\beta_1 N n + \beta_2 n^2, \tag{4}$$

where ν_i is the ionization collision frequency, ${U_x}^+$ and ${U_x}^{++}$ are the axial velocities of singly charged and doubly charged ions, β_0, β_1, β_2 and β_3 are the single, double, secondary and stepwise ionization collision rates accordingly, N^* is the excited neutrals density.

By neglecting of the electron inertia and azimuthal impulse convection terms in momentum equation projections solved together with the continuity equation, one can obtain the momentum equations in axial and azimuthal directions in the following form:

$$u_x = \mu_{eff}\left[-E_x - \frac{1}{en}\frac{\partial nT}{\partial x}\right], \tag{5}$$

$$u_\theta = u_x \frac{\omega}{(\nu_e+\nu_i)}, \tag{6}$$

where u_x and u_θ are the electron mean axial and azimuthal velocities accordingly, E_x is the axial electric field, T is the electron temperature measured in eV, e is the elementary charge, ω is the electron cyclotron frequency. The equation (5) contains the effective electron mobility μ_{eff}, which is defined as:

$$\mu_{eff} = \frac{e}{m\left(\frac{\omega^2}{\nu_e+\nu_i}+\nu_e+\nu_i\right)}, \tag{7}$$

where m is the electron mass. The equation (6) contains the total momentum transfer frequency ν_e, which is given by the following expression:

$$\nu_e = \beta_0 N + \beta_1 N + \beta_2 n + \beta_3 N^* + \beta_{elastic} N + \beta_{excit} N + \nu_{coulomb} + \nu_{ew} + \nu_{ano}, \tag{8}$$

where $\beta_{elastic}$ and β_{excit} are the elastic and excitation collision rates accordingly, ν_{columb}, ν_{ew} and ν_{ano} are the Coulomb, electron-wall and anomalous diffusion collision frequencies, determined as:

$$\nu_{ew} = \begin{cases} \frac{4}{3}\frac{1}{R-r}\sqrt{\frac{T}{M}}\frac{1}{1-\sigma}, x \le l \\ 0, \ x > l \end{cases}, \tag{9}$$

$$\nu_{ano} = \begin{cases} \frac{1}{160}\omega, x \le l \\ \frac{1}{40}\omega, x > l \end{cases}, \tag{10}$$

where R and r are outer and inner radiuses of the discharge chamber, l is the length of the discharge chamber, M is the ion mass, $\sigma = min(0.04T, 0.986)$ is the effective secondary electron emission (SEE) coefficient[13].

When the viscous stresses and the heat conduction are neglected, and the neutral excitation, stepwise, second, double ionization and wall losses are accounted, the electron energy equation could be written as follows:

$$\frac{\partial n\varepsilon}{\partial t} + \frac{\partial n u_x \varepsilon}{\partial x} = -n u_x e E_x - \frac{\partial u_x n T}{\partial x} - \beta_0\gamma_0 N n - \beta_1\gamma_1 N n - \beta_2\gamma_2 n^2 - \beta_3\gamma_3 N^* n - \beta_{excit}\gamma_{excit} N n - n P_{ew}, \tag{11}$$

where ε is the total electron energy, γ_0, γ_1, γ_2, γ_3 and γ_{excit} are the single, double, secondary, stepwise ionization losses and excitation losses accordingly, P_{ew} is the electron-wall energy loss rate obtained from the simplified theory of the presheath[13]:

$$P_{ew} = \nu_{ew}\left[2T + \frac{1}{2}m(u_x^2 + u_\theta^2) + (1-\sigma)e\Phi_w\right], \tag{12}$$

where $\Phi_w = \frac{T}{e} ln\left[\sqrt{\frac{M}{2\pi m}}(1-\sigma)\right]$ is the radial sheath potential .

Having combined the equations (1 – 6) with the electron energy equation (11), it is possible to obtain the final system of equations:

$$I_d = \frac{A}{\int \frac{1}{n\mu_{eff}}dx}\left\{e\Delta\phi_d + e\int \frac{(n_i^+ U_x{}^+ + n_i^{++} U_x{}^{++})}{n\mu_{eff}}dx + \int \frac{1}{n}\frac{\partial nT}{\partial x}dx\right\}, \tag{13}$$

$$u_x = \frac{n_i^+ U_x{}^+ + n_i^{++} U_x{}^{++}}{n} - \frac{I_d}{eAn}, \tag{14}$$

$$u_\theta = u_x \frac{\omega}{(\nu_e+\nu_1)}, \tag{15}$$

$$\left(\frac{\partial}{\partial t} + u_x\frac{\partial}{\partial x}\right)T = -T\nu_i + \frac{1}{3}m(2\nu_e+\nu_i)(u_x^2+u_\theta^2) - \frac{1}{3}mn\nu_e u_x{}^2,$$
$$-\frac{2}{3}\left[T\frac{\partial u_x}{\partial x} + \beta_0\gamma_0 N + \beta_1\gamma_1 N + \beta_2\gamma_2 n + \beta_3\gamma_3 N^* + \beta_{excit}\gamma_{excit} N + P_{ew}\right], \tag{16}$$

where A is the channel cross section.

A detailed derivation of the electron equation system (13-16) is presented in authors' previous work[9]. After solving the system of equations (13-16) with the heavy specious concentrations and velocities obtained from the PIC-step, one can obtain a nonsteady solution for Hall thruster discharge plasma. The system of equations was solved in this paper with the first order upwind scheme and with the following boundary condition for the electron temperature on the cathode boundary:

$$T|_{x=L} = 5\ eV, \tag{17}$$

where L is the simulation region length.

B Numerical model results

All the 19 operating modes of the KM-88 that we presented in the Tables 1-3 and 3 operating modes with different magnetic field gradient were modeled with 1D3V hybrid-PIC code. The simulations were conducted with a constant Bohm collision coefficient. The position of the maximum ion production rate (max Wi position) in the channel was conventionally taken as the position of the ionization region in the discharge channel. Moreover, the change in the acceleration region width was monitored to understand the trend in the plasma sheath shift. The authors construed the acceleration region as the region of the significant plasma potential drop, and, therefore, accepted the full width on half maximum (FWHM) of the electric field axial component E_x curve as the width of the acceleration region. The red arrow in the Fig. 3 shows the width of the plasma sheath. The step-like change of the electric field near the exit plane (*x=0* coordinate) is linked to the two region Bohm type of the electrical conductivity model. A sharp change in the effective collision frequency leads to an abrupt change of the plasma electric impedance, which causes a rapid electric field change. However, that fact does not affect the simulation results significantly, because more than 95% of ions appear upstream of the exit plane and do not lose their resulting velocity because of the chosen conductivity model.

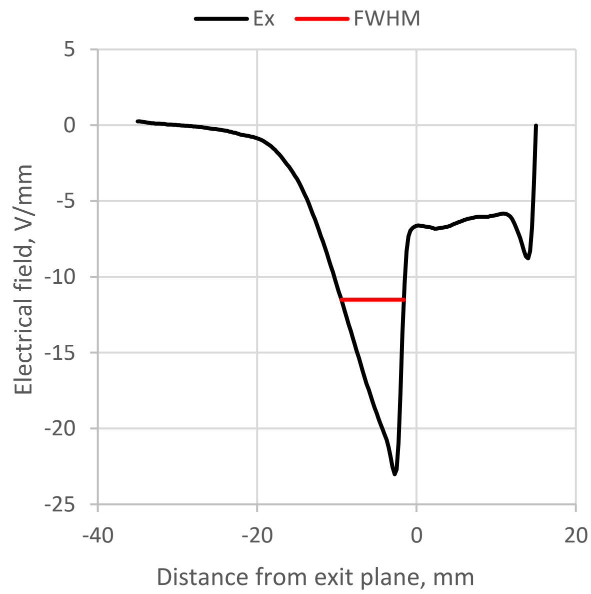

Figure 3. The plasma sheath width defined by authors in the paper.

Figures 4, 5 and 6 show the numerically obtained influence of the gas flow rate, magnetic field induction and discharge voltage on the plasma sheath location in the Hall thruster channel accordingly. The main ordinate axis in these figures illustrates the ion production rate and the second ordinate axis shows the electric field value. The curves on these figures were time-averaged over the interval of ~20 periods of the ionization mode after a quasi-stationary solution was obtained. The black arrows in the Fig. 4, 5 and 6 show the trend in the shift of the maximum ion production rate and in the electric field half-width change. Fig. 7, 8 and 9 present the FWHM of the electric field (main ordinate axis) and the maximum ion production rate position (second ordinate axis) dependencies on gas flow rate, magnetic field induction and discharge voltage accordingly.

Figures 4 and 7 indicate that the plasma sheath shifts downstream (away from the anode) when the gas flow rate increases within the throttle ratio of the KM-88 thruster. Additionally, these figures show the acceleration region contraction with the increase. The 1D3V numerical results presented in the Fig. 5 and 8 illustrate the acceleration region broadening and the plasma sheath shift inwards of the thruster channel (towards the anode) with the magnetic field increase. This shift leads to the thruster performance decrease and a more rapid ceramic insulators erosion. According to the 1D3V hybrid-PIC numerical simulations results presented in the Fig. 6 and 9 there is no explicit trend in the plasma sheath location change with the discharge voltage increase. The ionization region shifts upstream and the electric field FWHM is broadening when the discharge voltage increases from 250 to 450 V. However, along with the further discharge voltage growth up to 550 V the ionization region shifts back towards the exit plane and the electric field broadening nearly stops. Recall that the authors had assumed the Bohm coefficient to be fixed for all the simulation regimes, because of the lack of information about the electric conductivity dependence on thruster operating mode. It was highlighted in Ref. 9 that the Bohm type model for anomalous diffusion in a Hall thruster discharge can not guarantee full agreement of the simulation results with the experiment for the discharge voltage of 500 V. Consequently, the authors assume that the plasma sheath shift trend has changed because the Bohm type diffusion model became inapplicable in that area. In Section IV we will demonstrate that KM-88 discharge burning changes in the experiment when the discharge voltage exceeds 450 V.

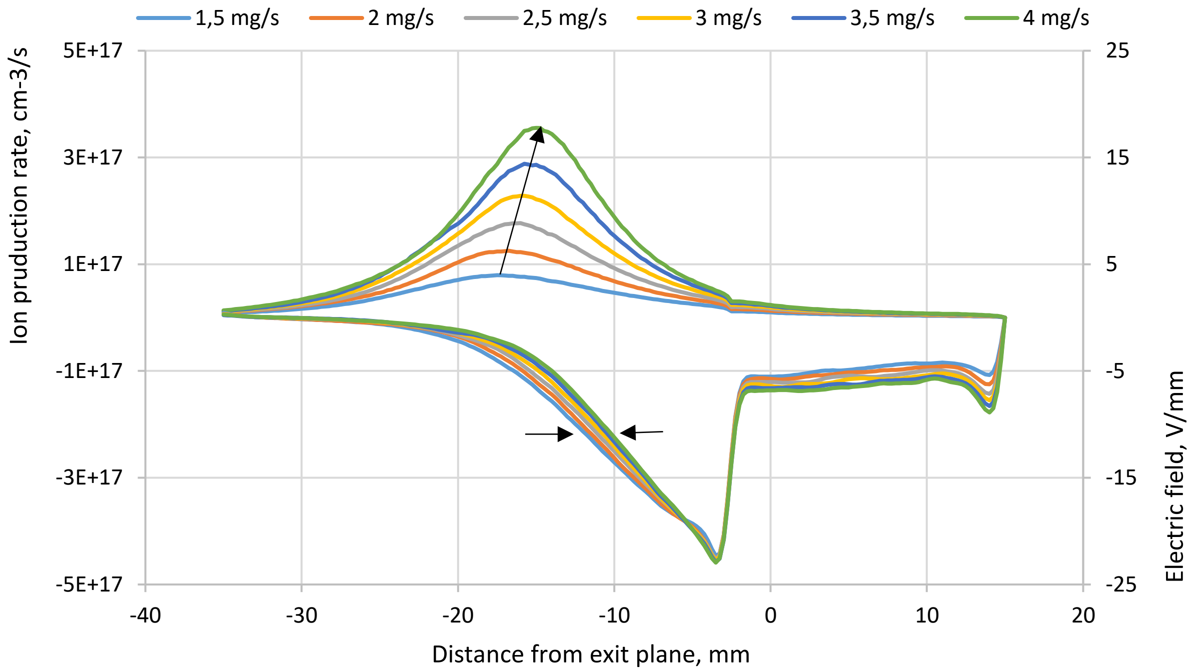

Figure 4. Plasma sheath shift with gas flow rate change.

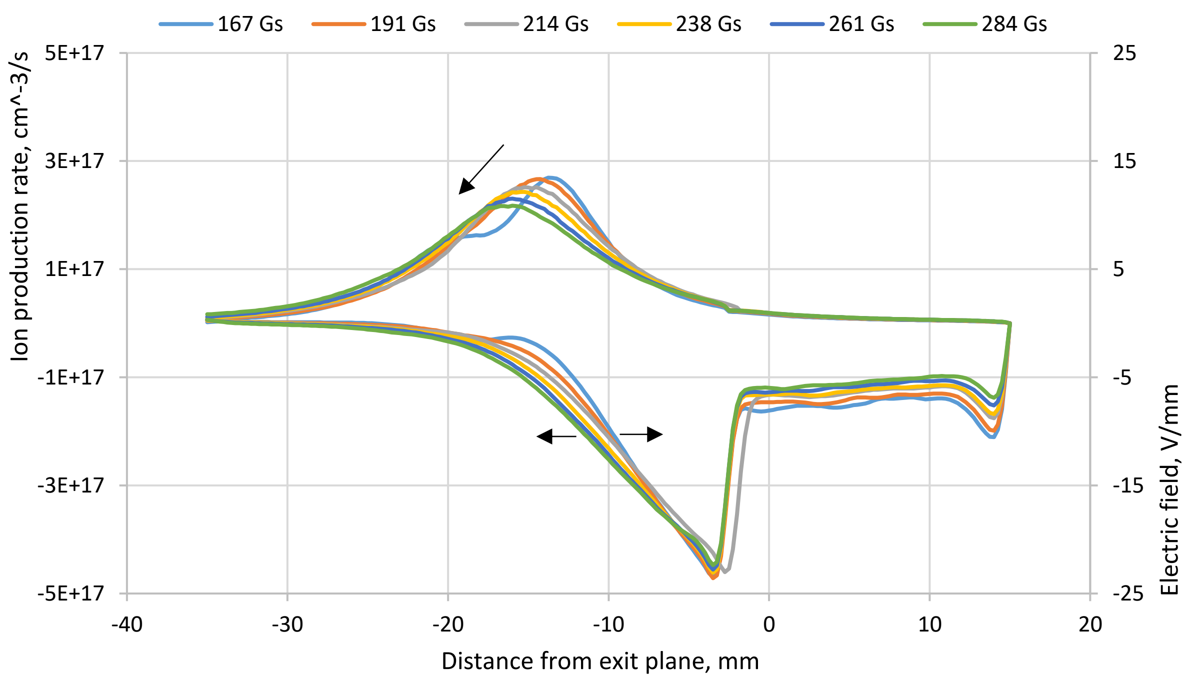

Figure 5. Plasma sheath shift with magnetic field change.

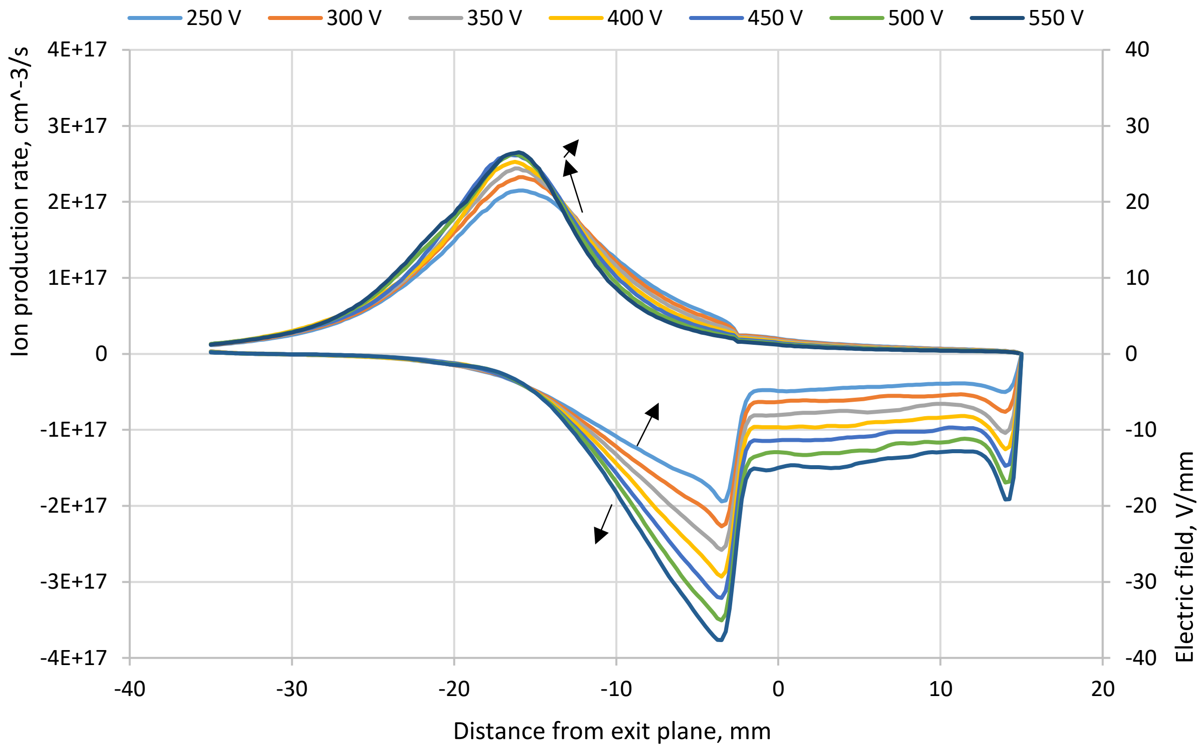

Figure 6. Plasma sheath shift with discharge voltage change.

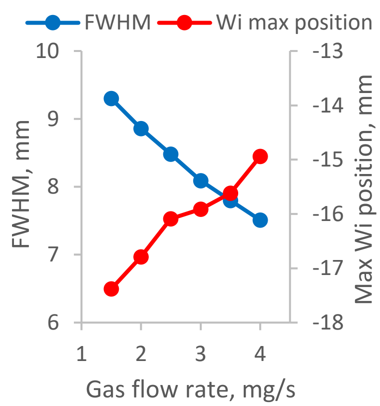

Figure 7. The FWHM of the electric field and dependence of the maximum ionization rate position on gas flow rate.

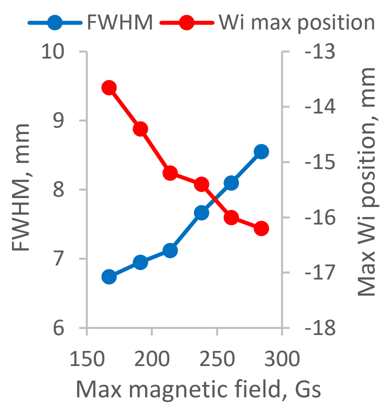

Figure 8. The FWHM of the electric field and dependence of the maximum ionization rate position on magnetic field induction.

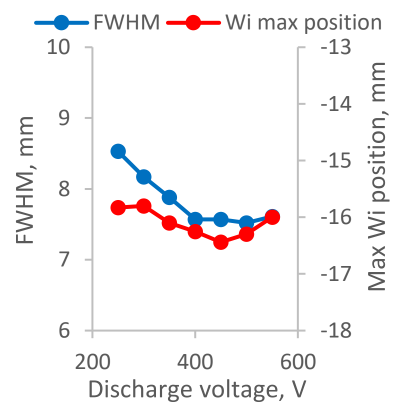

Figure 9. The FWHM of the electric field and dependence of the maximum ionization rate position on discharge voltage.

If Hall thruster is designed for space missions, it has mass restrictions. Therefore, the Hall thruster developers have to reduce the thruster's mass by minimizing the magnetic circuit mass. The reduction of the magnetic circuit mass leads to an increase in the magnetic flux density inside the circuits and their saturation. In such case, the gradient of the magnetic field inside of the Hall thruster channel reduces. The plasma sheath location dependence on the magnetic field gradient inside of the channel was numerically studied with 1D3V code. Figure 10 shows 3 magnetic field profiles with the same maximum and different gradients. The results of the calculations are presented in the Fig. 11. The main ordinate axis in the Fig. 11 illustrates the ion production rate; the second ordinate axis shows the magnetic field gradient and the electric field value. The solid lines above the zero level show the ion production rate, the solid lines under the zero level show the electric field and the dashed lines illustrate the magnetic field gradient. In the Fig. 11 one can see that a slight decrease in the magnetic field gradient causes a significant plasma sheath shift towards the anode and a broadening of the acceleration region. If one compares the influence of the maximum magnetic field change (Fig. 5) and the magnetic field gradient change (Fug. 11), one can conclude that the gradient of the magnetic field influences the plasma sheath location more prominently. In particular, by increasing the maximum magnetic field roughly twice, we shift the sheath by ~2,5 mm upstream; and by decreasing the magnetic field gradient by ~ 20%, we shift the sheath by ~4,3 mm upstream. The correlation between the ionization region location and the magnetic field gradient was observed earlier in 2D3V full-PIC simulations of the Hall thruster[14] and experimentally in Ref. 15. The authors in these works demonstrate that the maximum of the magnetic field gradient coincides with the ionization region location in radial direction and mention that the axial position of the acceleration sheath shifts at the same direction as the maximum of the magnetic field gradient. In this regard, the maximum of the ionization region should not shift with a uniform magnetic field increase (such an increase where the maximum magnetic field gradient remains constant). However, the numerous experimental data and simulation data in this paper testify that both the maximum magnetic field and the magnetic field gradient influence the plasma sheath location. Moreover, with the help of specifically chosen magnetic field distribution profiles the paper attests a prominent influence of the magnetic field gradient on the plasma sheath location.

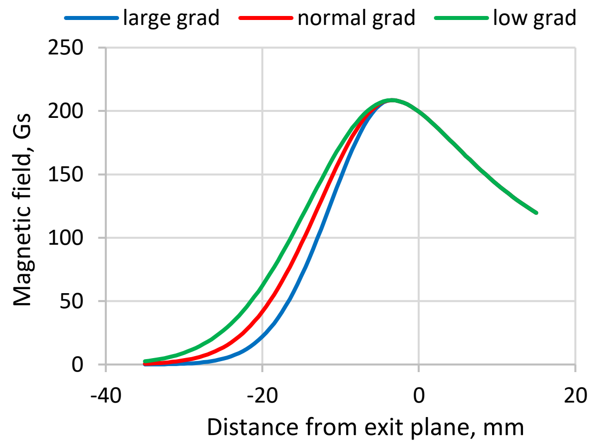

Figure 10. Middle line magnetic field with large, normal and low gradient inside of the channel.

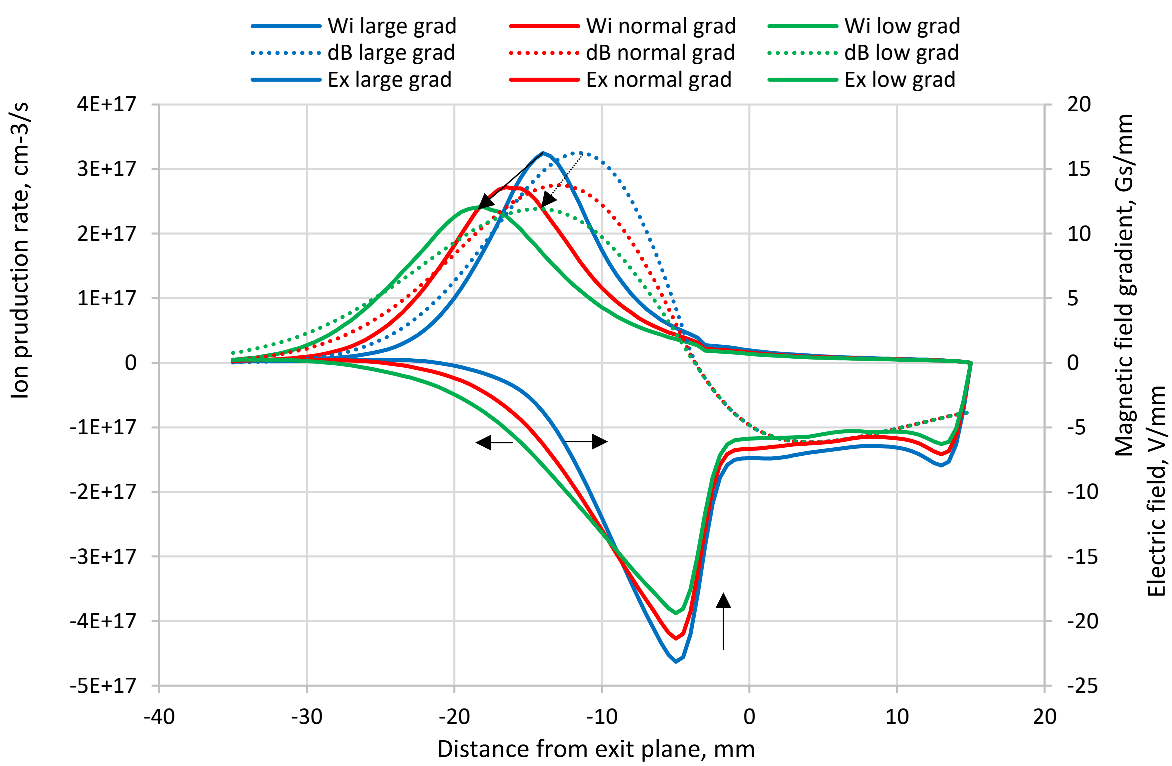

Figure 11. The trend of the plasma sheath location change with magnetic field gradient change.

IV. Validation and discussions

The tendencies obtained from the numerical investigation in Section III were validated with the results of the experiment described in Section II. The authors assumed the floating potential drop to have the same value both in the experiment and in the numerical simulations. That assumption was not proved experimentally in this work, but a corresponding examination is planned for the nearest future works. However, it is possible to show that the assumption is correct in the numerical simulations, and a more rapid floating potential drop corresponds to the plasma sheath shift towards the anode. Since the floating potential rather than the plasma potential was measured in the experiment, the numerically obtained plasma potential distributions should be recast into the floating potential distributions to ensure the comparison procedure is followed. The floating potential could be found from the condition of electron and ion current densities equality on the probe surface[16]:

$$\phi_{fl} = \phi + \frac{kT}{2e}\ln\left(\frac{\pi m}{2M}\right) \qquad (18)$$

where ϕ_{fl} is the floating potential, ϕ is the plasma potential, M is the xenon atom mass and k is the Boltzmann constant.

Figure 12 shows the numerically (solid lines) and experimentally (dashed lines) obtained floating potential distributions for various gas flow rates. Both investigations tell that the plasma sheath shifts downstream whenever the gas flow rate increases. To make the validation more informative the dependencies of the floating potential in the fixed coordinate *x=-4* mm are presented in the Fig 13. Seeing that the floating potential distributions curves do not cross each other all the way up to the exit plane, the tendencies seen in the fixed coordinate graph could be applied to the whole discharge channel region. The floating potential in the Fig. 13 rises in both numerical and experimental investigation with an increase in gas flow rate. In that case, the potential drop relocates downstream, which means that the plasma sheath shifts towards the exit plane. The maximum ionization rate location seen on the second ordinate axis in the Fig.13 confirms the described logic. As a result, the experimental data attest the numerical results described in Section III and the plasma sheath shifts towards the exit plane with the gas flow rate increase. All the rest experimental validations in this Section exploited the same logic.

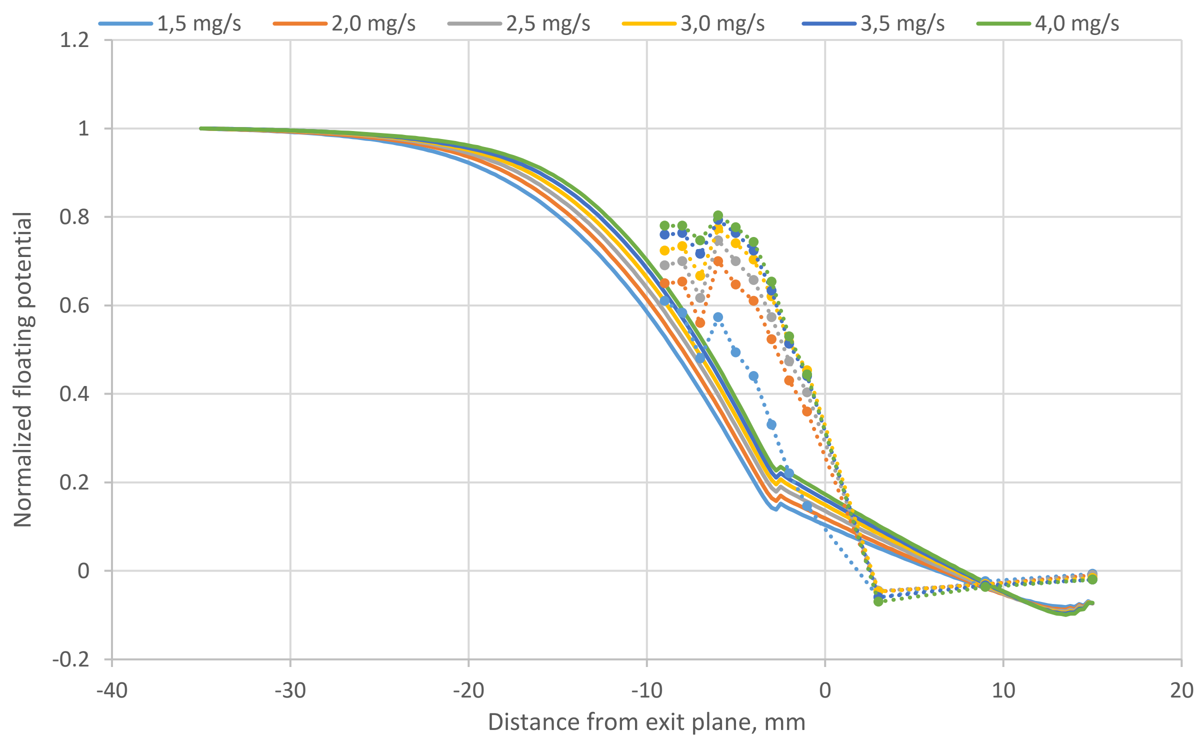

Figure 12. Normalized floating potential obtained numerically and experimentally with different gas flow rates.

The normalized floating potential distributions for several magnetic field induction values are presented in the Fig. 14. In accordance with the logic assumed in the previous paragraph, the numerical results tell us the sheath would always shift upstream with the magnetic field increase. However, the experimental results are not as linear as numerical ones. Figure 15 illustrates that the same trend in plasma sheath shift is observed in the experiment for the values of the maximum magnetic field on the middle line that are larger than 214 Gs. However, if the said magnetic field induction is lower than 214 Gs, the plasma sheath shifts towards the anode with the magnetic field decrease. The most probable reason for that could be the change in discharge operating mode. Figure 15 demonstrates that the amplitude of the discharge current oscillations in the operating mode with low magnetic field (dashed blue line) has a sharp increase when numerical investigation results for low magnetic fields (dashed orange line) have no significant growth of the oscillations rate.

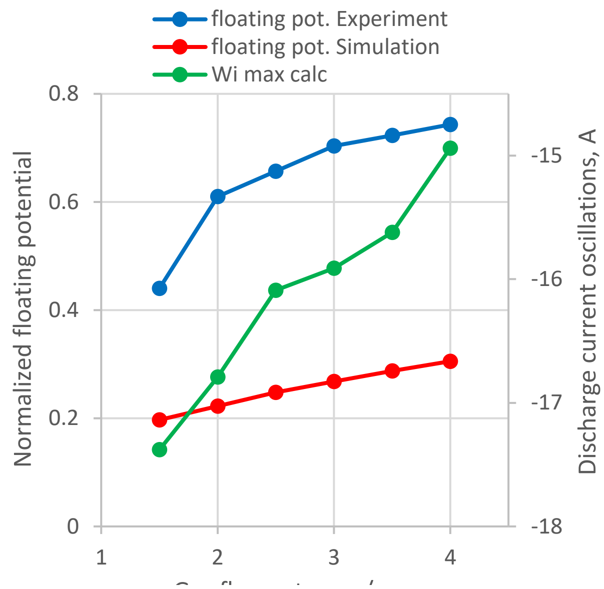

Figure 13. Position of the maximum ion production rate and the normalized floating potential at the point 4mm upstream from the exit plane for different gas flow rates.

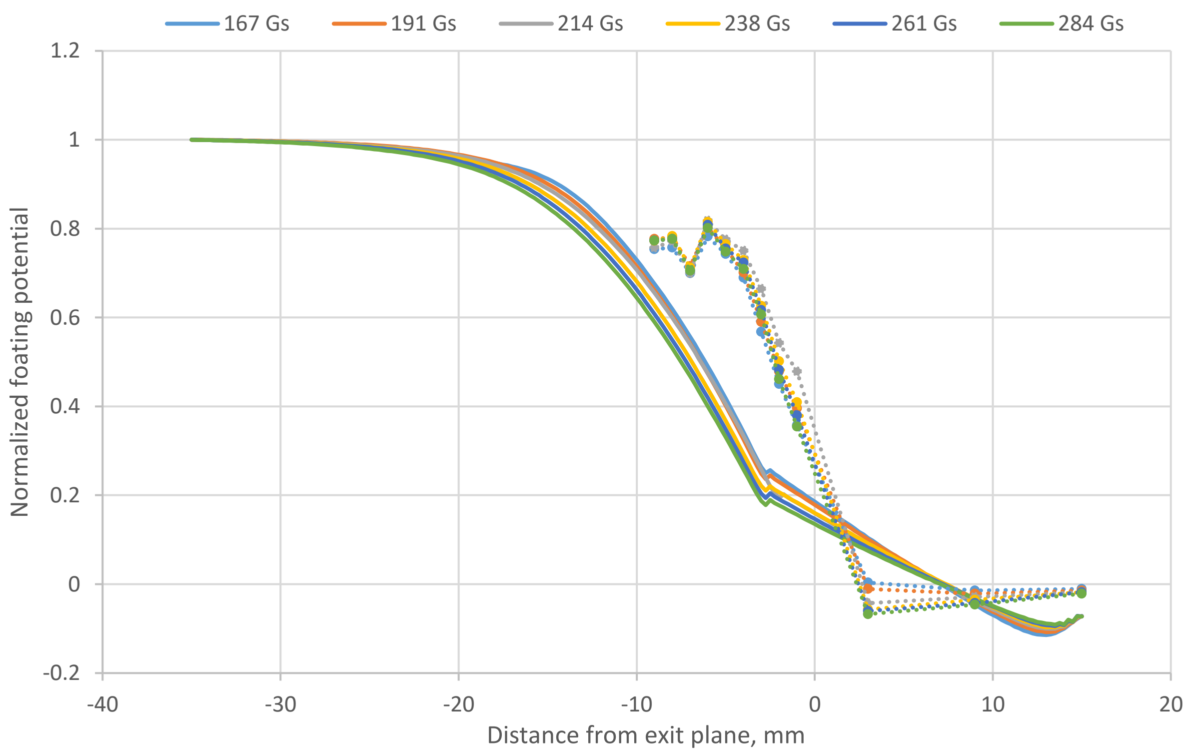

Figure 14. Normalized floating potential obtained numerically and experimentally with different magnetic fields.

Figure 16 represents the normalized floating potential obtained both in the experiment and in simulations for several discharge voltages. No obvious trends of the plasma sheath shift linked to the discharge voltage change were observed in both the experiment and the simulations. Figures 6 and 9 show that according to the simulation results the sheath shifts towards the anode when the discharge voltage rises up to 450 V. However, with the further increase in the discharge voltage the plasma sheath shifts back to the exit plane. With that, Fig. 17 illustrates that both in numerical and in experimental results the pace of growth of the discharge current oscillations amplitude changes. Moreover, the discharge oscillations spectrum has changed after the discharge voltage reached 450 V in the experiment. The most probable reason for the described effects could be the change in electric conductivity for high discharge voltages. The high frequency oscillations were observed in the oscillogram for the discharge voltages of 500 and 550 V. To the contrary, a Bohm type conductivity set in numerical investigation for all the discharge voltages cannot lead to such perturbations of the high frequency part of discharge current spectrum a priori.

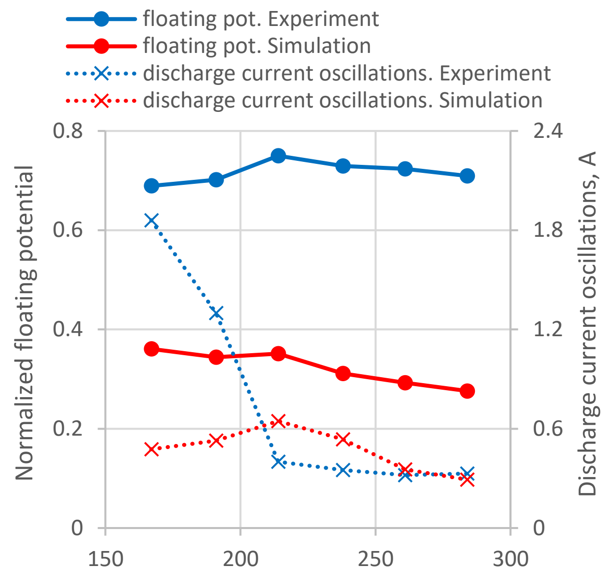

Figure 15. Normalized floating potential (main ordinate axis) and discharge current oscillations amplitude (second ordinate axis) in point with the coordinate *x=-4* mm with the different magnetic fields.

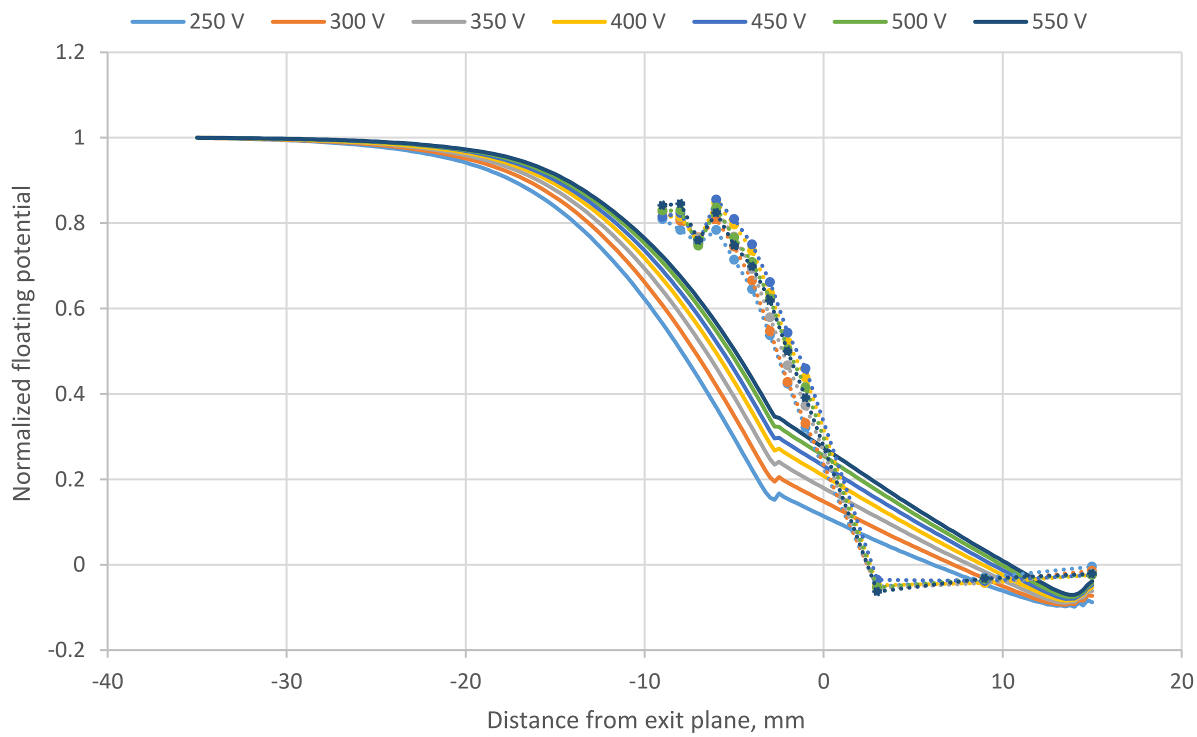

Figure 16. Normalized floating potential obtained numerically and experimentally with different discharge voltages.

V. Conclusion

Some tendencies in plasma sheath shift observed in the paper should be taken into consideration in magnetically shielded thrusters design:

- The plasma sheath shifts downstream with the gas flow rate increase when the thruster operates within the same oscillating regime;
- The plasma sheath shifts upstream and broadens with the magnetic field increase when the thruster operates within the same oscillating regime;
- The plasma sheath shifts downstream significantly with the magnetic field gradient increase when the thruster operates within the same oscillating regime;
- Significant influence of the oscillation regime on the plasma sheath location demands further investigation;
- The oscillation spectra changes in all frequencies with discharge voltage increase. Moreover, the plasma electric conductivity changes with oscillation spectrum and influences plasma sheath location in an unpredictable way: no certain trend in plasma sheath shift was observed.

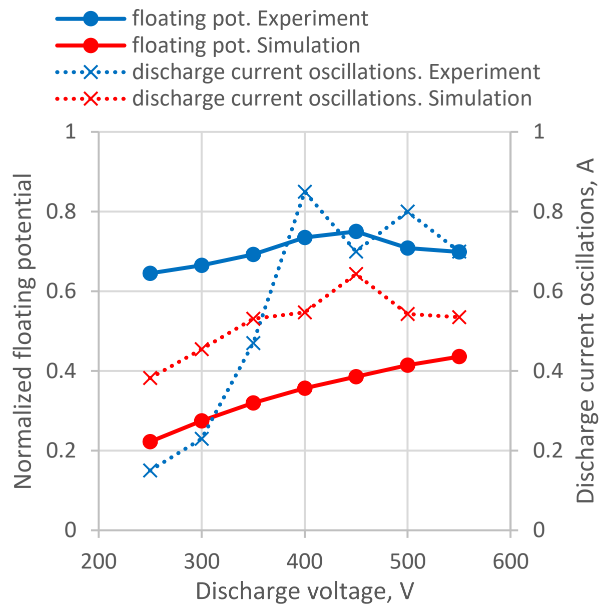

Figure 17. Normalized floating potential (main ordinate axis) and discharge current oscillations amplitude (second ordinate axis) in point with the coordinate *x=-4* mm with the different discharge voltage.

As a result, in authors' opinion, it is reasonable to reduce the magnetic field whenever gas flow rate should be increased within the discharge current throttle ratio for magnetically shielded Hall thrusters and vice versa. Since the tendency in the plasma sheath shift is opposite for the gas flow rate and the magnetic field, it is possible to find the proportion, which retains the plasma sheath position and saves the magnetic shielding effectiveness and consequently prolongs the thruster's lifetime in orbit. Along with that, it is reasonable to set up the restriction on the discharge current throttle ratio when the discharge voltage is constant: the gas flow rate could be reduced so far as the magnetic field induction allows to retain a stable oscillation regime. Furthermore, in accordance with 1D3V hybrid-PIC simulation results, it is reasonable to enhance the magnetic field gradient to achieve a more profitable magnetic shielding effect and reduce high-energy ions flux on the ceramics insulators. Finally, the discharge voltage change could lead to an unpredictable shift of the plasma sheath. Consequently, at least a short lifetime test should be passed for each discharge voltage within the discharge voltage throttle ratio to make sure that the plasma sheath location remains constant.

References

[1]Kim V., "Analysis of Erosion of insulator limiting the acceleration channel of CDPA," *Plasma sources and accelerators* , Vol. 6, 1982 (in Russian).

[2]Kim V., "Main physical features and processes determining the performance of stationary plasma thrusters," *Journal of propulsion and power*, Vol. 14, No. 5, September 1998.

[3]Semenkin A.V., "Investigation of erosion in anode layer thruster and elaboration high life design scheme," *23th International electric propulsion conference*, Seattle, 1993, pp. 93-231.

[4]Gris K., Mathers A., Walander B., and Khayms V., "Demonstration of 10,400 Hours of Operation on a 4.5 kW," *46th AIAA/ASME/SAE/ASEE Joint Propulsion Conference & Exhibit*, Nashville, 2010.

[5]Mikellides I.G., Katz I., Hofer R.R., and et al., "Magnetic Shielding of the Acceleration Cannel Walls in a Long-Life Hall Thruster," *46th AIAA/ASME/SAE/ASEE Joint Propulsion Conference & Exhibit*, Nashville, 2010, p. 6942.

[6]Hofer R., Kamhawi H., Herman D., and et al., "Development Approach and Status of the 12.5 kW HERMeS Hall Thruster for the Solar Electric Propulsion Technology Demonstration Mission," *Science 34th International Electric Propulsion Conference*, Hyogo, 2015, p. 186.

[7]Belikov M.B., Gorshkov O.A., Lovtsov A.S., and et al., "Probe Measurements in the Channel of 1.5 kW Hall Thruster with Discharge Voltage up to 1000 V," *30th International Electric Propulsion Conference*, Florence, 2007, p. 131.

[8]Gorshkov O.A., Ilyin A.A., and Rizakhanov R.N., "New Large Facility for High-Power Electric Propulsion Tests," *Proceedings of the 6th Propulsion for Space Transportation of the XXIst Century Symposium*, Versailles, 2002, p. S20_2.

[9]Shashkov A., Lovtsov A., and Tomilin D., "A one-dimensional with three-dimensional velocity space hybrid-PIC model of the discharge plasma in a Hall thruster," *Physics Of Plasmas*, March 2017, Vol. 24, p. 043501.

[10]Hara K., Boyd I.D., and Kolobov V.I., "One-dimensional hybrid-direct kinetic simulation of the discharge plasma in a Hall thruster," *Physics of Plasmas*, Vol. 19, 2012, p. 113508.

[11]Rostler P.S., "A 1-D Time-Dependent Model of a Hall Thruster with Sides Walls," *International electric propulsion conference*, 2001, pp. 01-22.

[12]Garrigues L., Boyd I.D., and Boeuf J.P., "Computation of Hall Thruster Performance," *Journal of propulsion and power*, Vol. 17, No. 4, July-August 2001.

[13]Barral S., Ahedo E., "Low-Frequency model of breathing oscillations in Hall discharges" *Physical Review*, Vol. 79, 2009, p. 046401.

[14]Irishkov S.V., Gorshkov O.A., and Shagayda A.A., "Fully Kinetic Modeling of Low Power Hall Thrusters," International Electric Propulsion Conference, 2005.

[15]Blinov N., Gorshkov O., and Shagayda A., "Experimental investigation of the magnetic field topology influence on structure of acceleration layer and performance of hall thrusters," 29th International Electric Propulsion Conference, 2005, pp. 2005-033.

[16]Huddlestone R, Leonard S, *Plasma Diagnostic Techniques.* New York-London: Academic Press, 1965, pp. 146